Journal of Analytical Science and Technology

RESEARCH ARTICLE Open Access

Adsorption of Cr(VI) onto cross-linked chitosan-almond shell biochars: equilibrium, kinetic, and thermodynamic studies

Türkan Altun[1*], Hüseyin Ecevit[1], Yakup Kar[2] and Birsen Çiftçi[3]

Abstract

In this study, to remove Cr(VI) from the solution environment by adsorption, the almond shell was pyrolyzed at 400 and 500 °C and turned into biochar (ASC400 and ASC500) and composite adsorbents were obtained by coating these biochars with chitosan (Ch-ASC400 and Ch-ASC500). The resulting biochars and composite adsorbents were characterized using Fourier transform infrared (FTIR) spectroscopy; Brunauer, Emmett, and Teller (BET) surface area; scanning electron microscopy/energy-dispersive X-ray spectroscopy (SEM/EDX); and the point of zero charge pH (pH_{pzc}) analyses. The parameters affecting the adsorption were examined with batch adsorption experiments and the optimum parameters for the efficient adsorption of Cr(VI) in 55 mg L^{-1} solution were determined as follows; adsorbent dosages: 5 g L^{-1} for biochars, 1.5 g L^{-1} for composite adsorbents, contact time: 120 min, pH: 1.5. It was seen that the temperature did not affect the adsorption much. Under optimum conditions, Cr(VI) adsorption capacities of ASC400, ASC500, Ch-ASC400, and Ch-ASC500 adsorbents are 11.33, 11.58, 37.48, and 36.65 mg g^{-1}, respectively, and their adsorption percentages are 95.2%, 97.5%, 94.3%, and 94.0%, respectively. Adsorption data were applied to Langmuir, Freundlich, Scatchard, Dubinin-Radushkevic, and Temkin isotherms and pseudo-first-order kinetic model, pseudo-second-order kinetic model, intra-particle diffusion model, and film diffusion model. The adsorption data fitted well to the Langmuir isotherm and pseudo-second-order kinetic models. From these results, it was determined that chemical adsorption is the dominant mechanism. Also, both intra-particle diffusion and film diffusion is effective in the adsorption rate. For all adsorbents, the Langmuir isotherm proved to be the most appropriate model for adsorption. The maximum monolayer adsorption capacities calculated from this model are 24.15 mg g^{-1}, 27.38 mg g^{-1}, 54.95 mg g^{-1}, and 87.86 mg g^{-1} for ASC400, ASC500, Ch-ASC400, and Ch-ASC500, respectively. The enthalpy change, entropy change, and free energy changes during the adsorption process were calculated and the adsorption was also examined thermodynamically. As a result, adsorption occurs spontaneously for all adsorbents.

Keywords: Adsorption, Cr(VI), Biochar, Chitosan, Almond shell, Pyrolysis

* Correspondence: turkanaltun@yahoo.com
[1]Department of Chemical Engineering, Konya Technical University, 42079 Konya, Turkey
Full list of author information is available at the end of the article

Springer Open

© The Author(s). 2021 **Open Access** This article is licensed under a Creative Commons Attribution 4.0 International License, which permits use, sharing, adaptation, distribution and reproduction in any medium or format, as long as you give appropriate credit to the original author(s) and the source, provide a link to the Creative Commons licence, and indicate if changes were made. The images or other third party material in this article are included in the article's Creative Commons licence, unless indicated otherwise in a credit line to the material. If material is not included in the article's Creative Commons licence and your intended use is not permitted by statutory regulation or exceeds the permitted use, you will need to obtain permission directly from the copyright holder. To view a copy of this licence, visit http://creativecommons.org/licenses/by/4.0/.

Introduction

The presence of potentially toxic elements, such as chromium, mercury, arsenic, cadmium, etc., in water is a factor that endangers the health of humans and all other living things. Wastewater produced by industrial activities plays the largest role in increasing concentrations of potentially toxic elements in water, if not managed correctly. Chromium is a toxic metal present in wastewater resulting from many industrial activities, particularly in the leather, electroplating, painting, and photography industries (Banerjee et al. 2017). Chromium exists in two different oxidation levels as Cr^{3+} and Cr^{6+} in aquatic environments. Both are of different physical and chemical properties. The human body needs low concentrations of Cr(III) for lipid, protein, and blood sugar metabolism (Bahador et al. 2021). Cr(VI) has carcinogenic, mutagenic, and teratogenic effects on living organisms and is highly toxic and harmful compared with Cr(III). Cr(VI) can accumulate in the liver, stomach, and kidneys, damaging the integrity and functions of cells (Foroutan et al. 2020). According to the World Health Organization guidelines, the concentration of Cr(VI) in drinking water is expected to be a maximum of 0.05 mg L^{-1} (Banerjee et al. 2017; Yüksel and Orhan 2019). The United States Environmental Protection Agency, on the other hand, has limited the maximum allowable total chromium concentration in drinking water to 0.1 mg L^{-1} (Bahador et al. 2021). Cr(VI) ions dissolved in water exist as oxyanions $HCrO_4^-$, CrO_4^{2-} and $Cr_2O_7^{2-}$ (Altun 2019).

Many methods, physicochemical, electrochemical, or based on advanced oxidation, have been proposed by researchers to remove Cr(VI) from water. These methods include chemical precipitation, membrane separation, ion exchange, adsorption, electrocoagulation, electrochemical reduction, electrodialysis, photocatalysis, and nanotechnologies. Among these, methods other than adsorption have disadvantages such as high cost, high energy requirement, complex and difficult operating conditions, and the production of a second waste after processing. Adsorption, on the other hand, is an efficient, cost-effective, and easy-to-use and reversible method when the appropriate solution, medium, and adsorbent are used (Abshirini et al. 2019; Imran et al. 2020; Peng and Guo 2020).

Many researchers are working on producing low-cost and effective adsorbents that can be used in Cr(VI) adsorption processes. For this purpose, Cr(VI) adsorption performances of many agricultural wastes were investigated in raw form or by applying various modifications to these wastes. Some of them include almond shell, almond shell-activated carbon, and almond shell biochar-supported zero-valent iron (Banerjee et al. 2017; Shu et al. 2020; Yüksel and Orhan 2019); peanut shell (Banerjee et al. 2017); cherry kernel shell, cherry kernel shell pyrolytic charcoal, and magnetic chitosan-coated cherry kernel shell pyrolytic charcoal (Altun 2019; Altun and Ecevit 2020); apricot stone-activated carbon (Yüksel and Orhan 2019); peach stone activated carbon (Yüksel and Orhan 2019); *Moringa oleifera*-activated carbon and its composites with chitosan and Fe_3O_4 (Bahador et al. 2021); magnetite- and HNO_3-modified quinoa residues biochar (Imran et al. 2020); chitosan-modified magnetic bamboo residues biochar (Zhang et al. 2020); zero-valent iron-supported rice straw biochar (Qian et al. 2017), porous carbon derived from corn straw (Ma et al. 2019); magnetic biochar derived from *Melia azedarach* wood (Zhang et al. 2018); and magnetic biochar derived from pinewood sawdust (Yang et al. 2017).

The cost of the adsorption process is significantly reduced by the assessment of agricultural wastes as adsorbents. However, some modifications should be made to these wastes in order to increase the adsorption efficiency of agricultural wastes in some processes. These modifications can be by means of chemically modifying the waste, transforming it into biochar by pyrolysis, or compositing it by blending it with various matrices and additives (Shu et al. 2020; Xiao et al. 2019; Yüksel and Orhan 2019; Zhang et al. 2020).

Natural polysaccharides such as chitosan, chitin, and cellulose are frequently used in economic, medical, and environmental applications due to their unique structure and properties, being biocompatible and biodegradable (Foroutan et al. 2020). Chitosan, which is frequently used as a matrix in composite adsorbents, is a polysaccharide obtained by deacetylating chitin and Cr(VI) adsorption capacity of it is high because it contains hydroxyl (-OH) and amino ($-NH_2$) groups. However, stability at acidic pHs, thermal stability, and mechanical resistance of chitosan are low. These disadvantages make the use of chitosan as an adsorbent difficult. Therefore, it is a better option to blend chitosan with various additives into a composite and treat it with a crosslinking agent such as glutaraldehyde (Dandil et al. 2019; Sargın and Arslan 2015).

In this study, the almond shell, the base material of the adsorbents tested for adsorption of Cr(VI), is an agricultural waste produced in large quantities. In the previous study, the maximum Cr(VI) adsorption capacity of raw almond shell was found to be 3.40 mg g^{-1} (Pehlivan and Altun 2008). In the literature, there are studies in which almond shell and almond shell biochars are used as adsorbents for the removal of various organic and inorganic contaminants (Ahsaine et al. 2018; Duran et al. 2011; Rai et al. 2018). However, there is no study examining the effects of coating almond shell biochar with chitosan on Cr(VI) removal. In the study, biochar was obtained by pyrolysis of almond shells at 400 °C and 500 °C and composite beads were synthesized by coating

with chitosan. The efficiency of the obtained biochar and composite adsorbents for the removal of Cr(VI) was examined.

Materials and methods

Materials

In this study, almond shells were purchased from local vendors in Konya/Turkey. Two different biochar adsorbents were obtained by pyrolyzing almond shells at 400 °C and 500 °C temperatures (ASC400 and ASC500) with a heating rate of 10 °C min^{-1} under nitrogen flow (100 mL min^{-1}).

All the chemicals used in the study are of analytical grade. Chitosan and glutaraldehyde were purchased from Sigma-Aldrich. Potassium dichromate, acetic acid, sodium hydroxide, hydrochloric acid, and ethanol were purchased from Merck. All solutions were prepared with ultrapure water supplied by Direct-Q® UV Water Purification System.

Preparation of composite adsorbents

The coating of ASC400 and ASC500 adsorbents with chitosan was conducted by using the following method suggested by Sargın et al. (2015): First, ASC400 and ASC500 adsorbents were ground with a Retsch RM 100 grinder and sieved with a Retsch AS 200 sieve shaker to make the particle size less than 125 μm. Three grams of chitosan was added to 150 mL of 3 wt.% acetic acid solution and mixed for 24 h. Then, 1.5 g of biochar was added to this mixture and mixed for a further 2 h. The resulting liquid mixture was dropped into a 3 M 250 mL NaOH solution to form beads. The beads were left in the solution overnight to harden, and then separated from the solution and washed until pH 7. The washed beads were mixed in a solution containing 30 mL of ethanol and 0.3 mL of glutaraldehyde at 70 °C for 5 h, and the chitosan in the beads was crosslinked with glutaraldehyde. The beads were then filtered and washed with ethanol to remove unreacted glutaraldehyde, then washed with ultrapure water until pH 7 and dried at room temperature for 24 h. The cross-linking reaction between chitosan and glutaraldehyde is given in Fig. A.1. These processes were performed for both ASC400 and ASC500, and chitosan-almond shell biochar (Ch-ASC400 and Ch-ASC500) adsorbents were obtained.

Characterizations of adsorbents

The adsorbents were characterized by using various methods to determine their physical and chemical properties. The characterizations of adsorbents were made with Fourier transform infrared (FTIR) spectroscopy (Bruker Vertex 70); Brunauer, Emmett, and Teller (BET) surface analysis (Quantachrome QuadraWin); and scanning electron microscopy/energy-dispersive X-ray spectroscopy (SEM/EDX) (Hitachi – SU 1510). In addition, the point of zero charge pHs (pH_{pzc}) of the adsorbents were determined. The pH_{pzc} value indicates the charge of the adsorbent surface. When pH < pH_{pzc}, the adsorbent surface is positively charged, and when pH > pH_{pzc}, the adsorbent surface is negatively charged. For the determination of pH_{pzc}, 0.1 M NaCl solutions at different pH (2-12) were prepared. The pHs of the solutions was adjusted with 0.1 M HCl and NaOH solutions. Then, 25 mL of NaCl solution and 0.05 g of the adsorbent were mixed at 150 rpm for 36 h. The final pHs (pH_f) of the solutions was measured at the end of the contact period. pH_i values versus $pH_f - pH_i$ (ΔpH) values were plotted and the point where the graph intersected the pH_i-axis was determined as pH_{pzc} (Stoia et al. 2017).

Batch scale adsorption experiments of Cr(VI)

The adsorption efficiencies of Cr(VI) of the prepared ASC400, ASC500, Ch-ASC400, and Ch-ASC500 adsorbents were investigated by batch adsorption experiments. Cr(VI) solutions in various concentrations to be used in adsorption experiments were prepared by diluting 260 mg L^{-1} Cr(VI) stock solution in appropriate proportions. The Cr(VI) stock solution was prepared by dissolving the 735.5 mg potassium dichromate ($K_2Cr_2O_7$) salt in 1 L ultrapure water. As a result of the experiments, the effects of adsorbent dosage (0.5-12 g L^{-1}), Cr(VI) initial concentration (10–175 mg L^{-1}), pH (1.5–7), temperature (25–55 °C), and contact time (10–240 min) parameters on adsorption were investigated and optimum adsorption conditions were determined. In the experiments, 5 mL of Cr(VI) solution and adsorbents were mixed at 200 rpm for a certain contact time, and at the end of this period, the adsorbent was filtered off from the solution. Finally, the concentration of Cr(VI) in the resulting solution was analyzed by using a UV-visible spectrophotometer (Shimadzu UV-1700) at the maximum absorption wavelength of 349 nm. In addition, using the data obtained from these studies, the suitability of isotherm and kinetic models for adsorption was examined and the thermodynamic parameters of adsorption were calculated. With the help of these calculations, the adsorption mechanism was clarified.

Measurement of adsorption performance

The adsorption capacity (q_e, mg g^{-1}) and the adsorption efficiency (% adsorption) were calculated using Eqs. 1 and 2, respectively.

$$q_e = \frac{(C_0 - C_e)V}{w} \quad (1)$$

$$\%\text{adsorption} = \frac{C_0 - C_e}{C_0} \times 100 \quad (2)$$

where C_0 and C_e are Cr(VI) concentrations (mg L^{-1}) at the beginning and end of the contact time, respectively,

V is the solution volume (L), and w is the mass of adsorbent (g).

Equilibrium and kinetic models

Adsorption equilibrium data were applied to Freundlich (Eq. 3), Langmuir (Eq. 4), Scatchard (Eq. 5), Dubinin-Radushkevich (D-R) (Eqs. 6 and 7), and Temkin (Eq. 8) isotherm models. The kinetic data of adsorption were applied to pseudo-first-order kinetic (Eq. 9), pseudo-second-order kinetic (Eq. 10), intra-particle diffusion (Eq. 11), and film diffusion (Eq. 12) models. The linearized equations of these models are given in the following equations. By placing the adsorption data in these equations, the determination coefficient (R^2) values for each model were calculated from the results obtained. The magnitudes of these determination coefficient values, which have a value between 0 and 1, show how compatible the adsorption is to that model (Yang et al. 2017). Also, the data in the Intra-particle diffusion model equation is divided into two separate parts. The fact that the graphics pass through the origin shows the compatibility of this model. The fact that the line in the film diffusion model graphic does not pass through the origin, however, indicates the compatibility of the model (Oussalah et al. 2019). Accordingly, the assumptions of the model with which the adsorption is compatible are accepted as valid for this adsorption process and the adsorption mechanism has been elucidated.

$$\log q_e = \log K_F + \frac{1}{n}\log C_e \tag{3}$$

$$\frac{C_e}{q_e} = \frac{C_e}{A_s} + \frac{1}{A_s K_b} \tag{4}$$

$$\frac{q_e}{C_e} = Q_s K_s - q_e K_s \tag{5}$$

$$\ln q_e = \ln X_m - K\varepsilon^2 \tag{6}$$

$$E = (2K)^{-1/2} \tag{7}$$

$$q_e = \frac{RT}{b}\ln A_T + \frac{RT}{b}\ln C_e \tag{8}$$

where K_F is the Freundlich model constant regarding the adsorption capacity, n is the heterogeneity factor, A_s and Q_s are the maximum monolayer adsorption capacities, K_b is Langmuir bonding term related to interaction energies, K_s is the binding constant, ε is the Polanyi potential, X_m is the maximum adsorption capacity of adsorbent, K is the adsorption energy constant of D-R model, E is the adsorption energy, b is the Temkin constant associated with the heat of adsorption, A_T is the equilibrium binding constant, R is the universal gas constant (8,314 J $mol^{-1}K^{-1}$), and T is the temperature.

$$\log(q_e - q_t) = \log q - \left(\frac{k_{ad} t}{2.303}\right) \tag{9}$$

$$\frac{t}{q_t} = \frac{1}{k_2 q^2} + \left(\frac{1}{q}\right)t \tag{10}$$

$$q_t = K_i \times t^{0.5} + C \tag{11}$$

$$-\ln\left(1 - \frac{q_t}{q_e}\right) = k_{fd} t \tag{12}$$

where t is contact time; q_t is the experimental adsorption capacity at time t; q is the calculated equilibrium adsorption capacity; k_{ad}, k_2, K_i, and k_{fd} are the rate constants of pseudo-first-order adsorption, pseudo-second-order adsorption, intra-particle diffusion, and liquid film diffusion, respectively; and C is the constant related to the boundary layer thickness.

Adsorption thermodynamics

The changes of enthalpy (ΔH), entropy (ΔS) and Gibbs free energy (ΔG), and thermodynamic equilibrium constant (K_D) of adsorption were calculated by using the results obtained from the experiments in which the effect of temperature on adsorption was determined. These results were later used in the interpretation of the adsorption mechanism. These values are calculated with the help of Eqs. 13, 14, and 15 given below (Kołodyńska et al. 2017).

$$K_D = \frac{q_e\ (\text{mmol g}^{-1}) \times w\ (g)}{C_e\ (\text{mmol } mL^{-1}) \times V\ (mL)} \tag{13}$$

$$\log K_D = \frac{0.434}{R}\Delta S - \frac{0.434}{RT}\Delta H \tag{14}$$

$$\Delta G = \Delta H - T\Delta S \tag{15}$$

Effect of presence of Cl^- ion

Industrial wastewater may contain many ions that may affect the adsorption efficiency. In order to determine this effect, adsorption experiments were carried out with solutions containing 0.1 M and 0.2 M Cl^- ion under optimum conditions and the results were noted.

Results and discussion

Characterizations of adsorbents

FTIR spectra of ASC400, Ch-ASC400, ASC500, and Ch-ASC500 before and after Cr(VI) adsorption processes are shown in Fig. 1 and Fig. 2.

According to the FTIR spectra in Fig. 1 and Fig. 2, the band between 3300 and 3350 cm^{-1} indicates the N-H and O-H stretching vibrations (Dewage et al. 2018). The band around 2915 cm^{-1} indicates the stretching of sp^3 hybridization of the C-H bond (Dewage et al. 2018). The

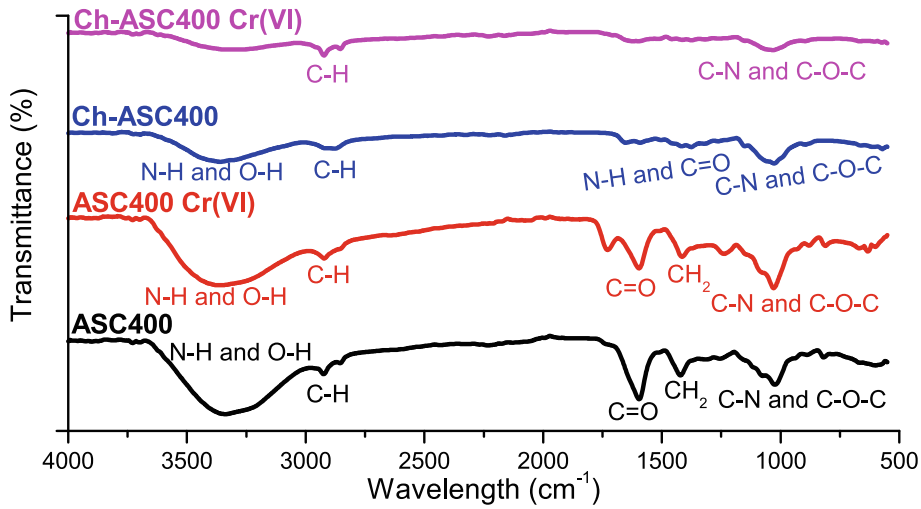

Fig. 1 FTIR spectra of ASC400 and Ch-ASC400 before and after Cr(VI) adsorption

band around 1590 cm^{-1} indicates the C=O stretching of the carboxyl group. The occurrence of two separate peaks in this interval after coating with chitosan indicates amide formation. The band with a smaller wavelength than these peaks indicates the vibrations of the groups that can be named as amide 1 (C=O stretching) and the band with large wavelengths as amide 2 (N-H bending) (Liu et al. 2017). The band in the range of 1365–1403 cm^{-1} shows CH_2 stretching vibrations (Xiao et al. 2019). The band in the range of 1012–1022 cm^{-1} indicates the C-N aliphatic amine and C-O-C groups (Xiao et al. 2019; Zhang et al. 2020). The band between 800 and 940 cm^{-1} indicates N-H wagging vibrations (Dewage et al. 2018). When the spectra are examined, it is seen that the functional groups in the ASC500 structure are less than those in the ASC400 structure. This shows that the carbonization is higher due to the higher temperature pyrolysis of the material. After the adsorption of Cr(VI), it is observed that the intensity of the bands indicating N-H, O-H, CH_2, C-N, C-O-C bonds decrease. This situation indicates that Cr(VI) is adsorbed to the surface by means of these groups.

According to BET surface area analysis, the specific surface areas of ASC400, ASC500, Ch-ASC400, and Ch-ASC500 are 275.6, 256.8, 8.0, and 9.1 m^2 g^{-1}, respectively.

SEM images of biochars and composite adsorbents are given in Fig. 3 and Fig. 4, respectively. EDX analysis results of biochars and composite adsorbents are given in Fig. 5 and Fig. 6 respectively.

It is seen in SEM images that the surfaces of the composites formed after the biochars are coated with

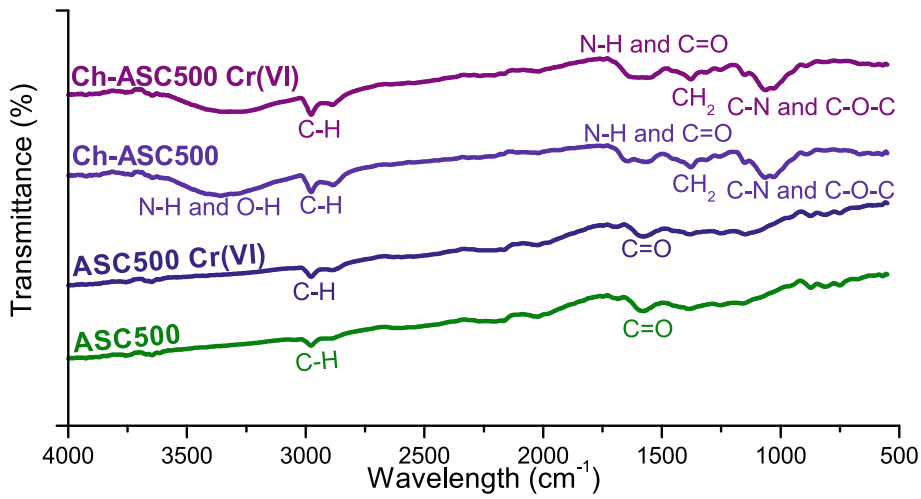

Fig. 2 FTIR spectra of ASC500 and Ch-ASC500 before and after Cr(VI) adsorption

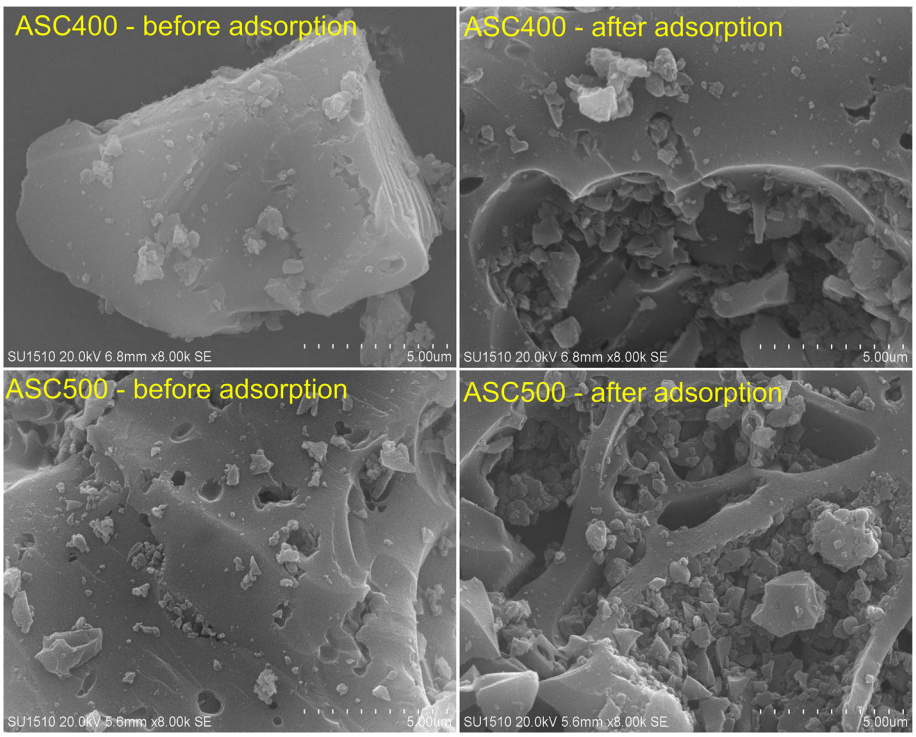

Fig. 3 SEM images of ASC400 and ASC500 before and after Cr(VI) adsorption

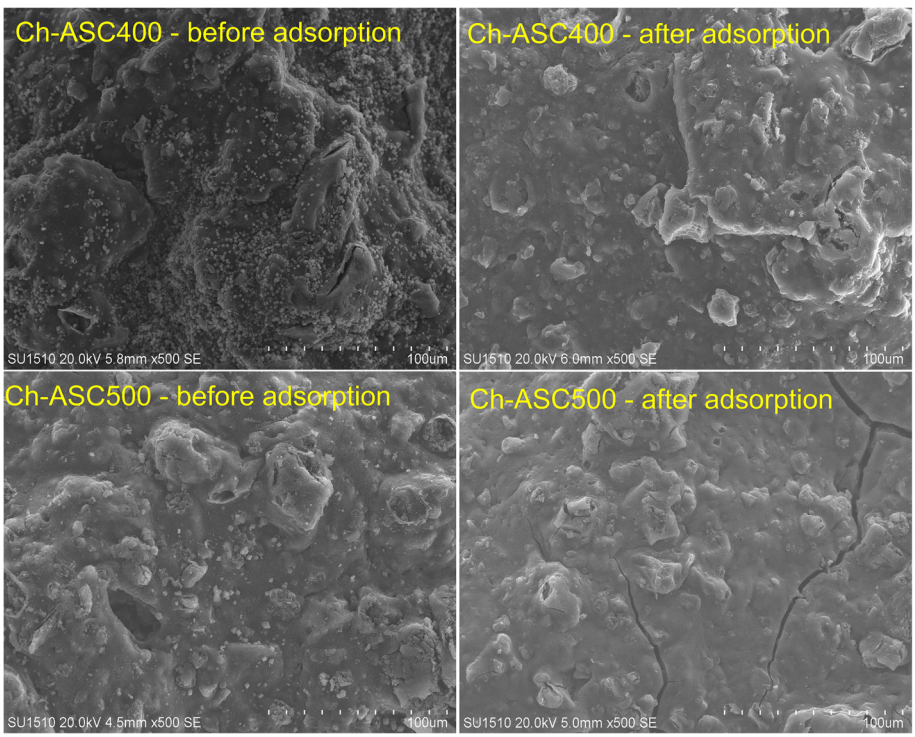

Fig. 4 SEM images of Ch-ASC400 and Ch-ASC500 before and after Cr(VI) adsorption

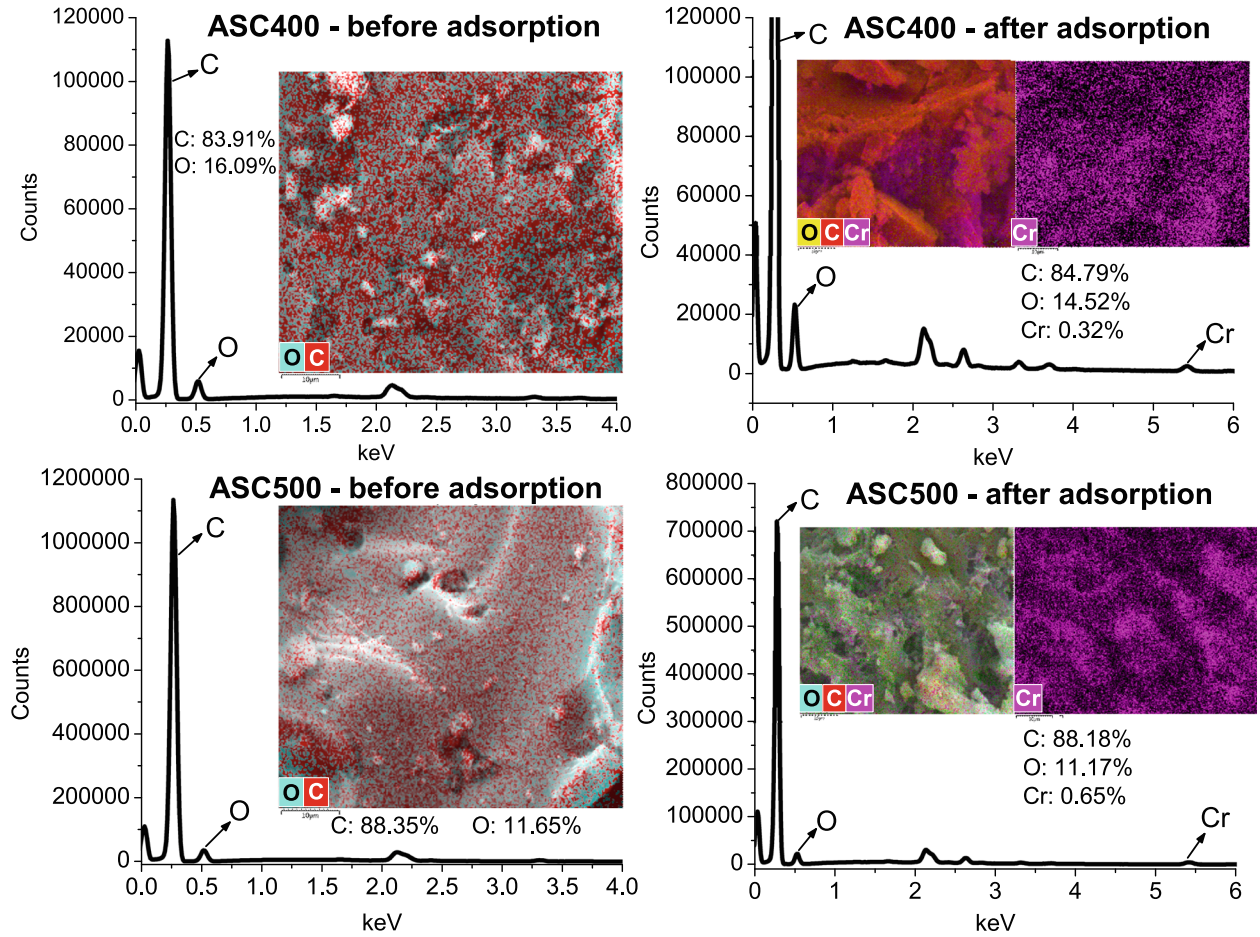

Fig. 5 EDX spectra and elemental mapping images of ASC400 and ASC500 before and after Cr(VI) adsorption

chitosan are smooth and homogeneous, that is, the biochars and chitosan are well distributed on the surfaces. In addition, forming of large particles and filling of the gaps on the surfaces after Cr(VI) adsorption supports the conclusion that Cr(VI) is adsorbed by adsorbents.

The elements on the surfaces of the adsorbents before and after the Cr(VI) adsorption are shown by means of EDX spectra and elemental mapping images in Fig. 5 and Fig. 6. These results prove that Cr(VI) is adsorbed on the surface of the adsorbents. Also, as shown in Fig. 5 and Fig. 6 Cr is uniformly displayed on the surfaces of all adsorbents.

The electrical charges of adsorbents are positive in solution environments with lower pH than pH_{pzc} values, but negative in solution environments with higher pH. pH_{pzc} graphics are given in Fig. A.2. Here, the points where the graphs intersect the x-axes show the pH_{pzc} values of the adsorbents. The pH_{pzc} of ASC400 and ASC500 is 7.38, the pH_{pzc} of Ch-ASC400 is 7.45, and the pH_{pzc} of Ch-ASC500 is 7.54. Accordingly, it was understood that the biochar synthesis temperature did not have a significant effect on pH_{pzc}. pH_{pzc} values are very important for adsorption processes. This information makes it easy to comment on electrical interactions in the adsorption process (Liu et al. 2017).

Effect of adsorbent dosage on Cr(VI) adsorption

The change of adsorption percentage and adsorption capacity values against the adsorbent dosage is graphically shown in Fig. 7.

Adsorbent dosage is a parameter that has a significant effect on adsorption. Increasing the adsorbent dosage increases the adsorption percentage but decreases the adsorption capacity. This prevents the efficient use of the adsorbent (Parlayıcı 2019). The reason for the increase in the adsorption percentage with the increase of the adsorbent dosage may be due to the increase in the active sites where the oxyanions containing Cr(VI) can be attached. On the other hand, the reason for the decrease in adsorption capacity with increasing adsorbent dosage may be the decrease in Cr(VI) concentration corresponding to adsorbent active sites at high adsorbent dosages (Esvandi et al. 2020). According to the results of the experiments, an adsorbent dosage value that gives an

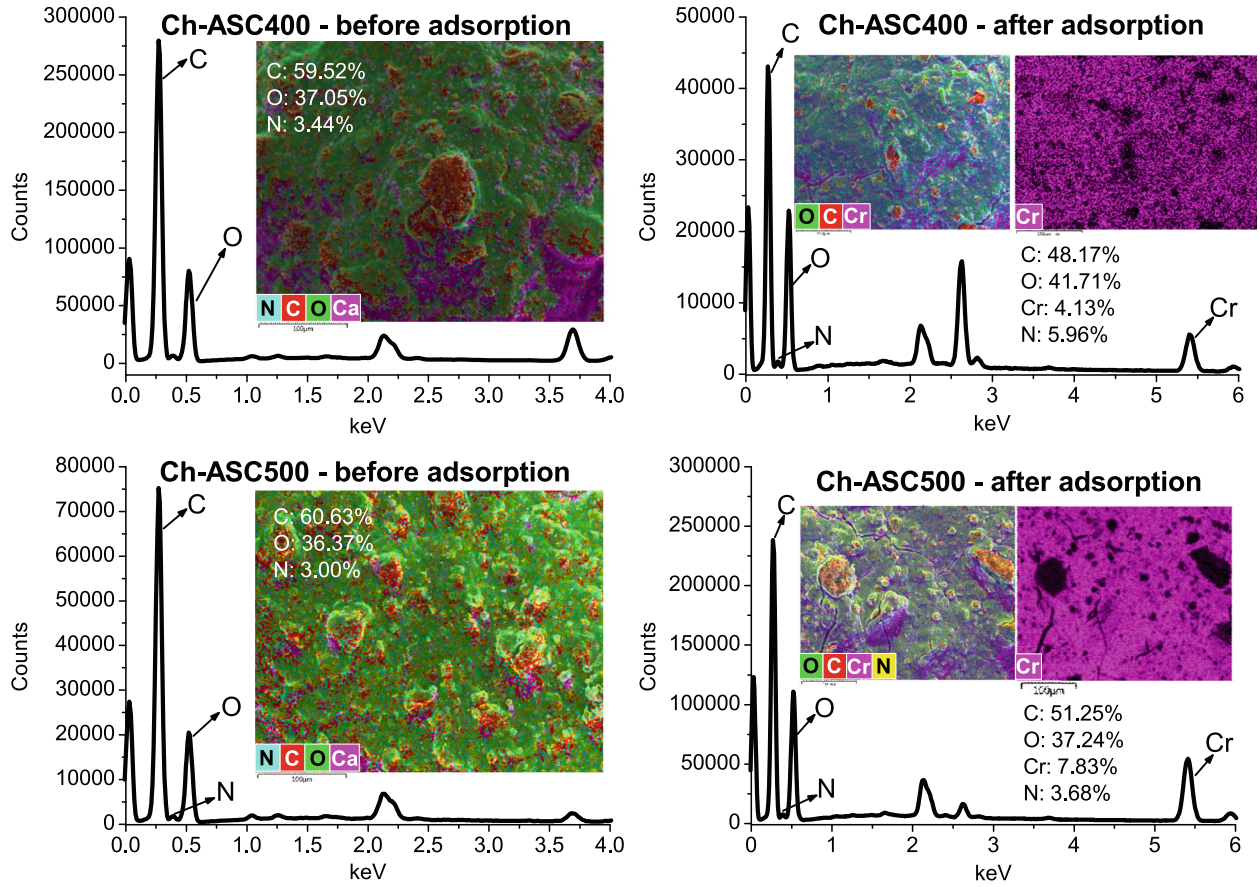

Fig. 6 EDX spectra and elemental mapping images of Ch-ASC400 and Ch-ASC500 before and after Cr(VI) adsorption

optimum result between the adsorption capacity and the adsorption percentage was determined. These dosages are 5 g L^{-1} for ASC400 and ASC500, and 1.5 g L^{-1} for Ch-ASC400 and Ch-ASC500.

Effect of initial Cr(VI) concentration on Cr(VI) adsorption

The effect of the initial Cr(VI) concentration on adsorption can be seen in Fig. 8.

As seen in Fig. 8, the initial Cr(VI) concentration is a parameter that significantly affects the adsorption. As the initial Cr(VI) concentration increases, the adsorption percentage decreases, on the other hand, the adsorption capacities of the adsorbents increase. For this reason, an optimum concentration value should be determined for these two values in experimental studies. In this study, 55 mg L^{-1} was determined as the optimum concentration.

Adsorption equilibrium

The adsorption equilibrium was modeled by using the data of changes in adsorption capacity versus the initial Cr(VI) concentration. For this purpose, the compatibilities of Freundlich, Langmuir, Scatchard, Dubinin-Radushkevic (D-R), and Temkin isotherms to adsorption data were investigated. The determination coefficients (R^2) and other model constants of these isotherm models are shown in Table 1.

Isotherm models are useful and necessary to elucidate the adsorption mechanism. By examining the compatibility of the data of an adsorption process with the calculations of the isotherm models, it can be understood how valid the assumptions of the relevant model are for the adsorption process. Accordingly, the following conclusions can be drawn from the data in Table 2: The high R^2 values of the Langmuir and Freundlich isotherms indicate that both physical and chemical binding occurs in adsorption (Brion-Roby et al. 2018; Freundlich 1907; Langmuir 1916). However, the fact that the R^2 values of the Langmuir isotherm are slightly higher than the R^2 values of the Freundlich isotherm indicates that chemical adsorption is more dominant (Brion-Roby et al. 2018; Langmuir 1916). The R^2 values of the Scatchard isotherm also support this comment (Brion-Roby et al. 2018). E values calculated using the D-R model are in the range of 8–16 kJ mol^{-1} for all adsorbents, indicating that chemical adsorption is more dominant (Hu and

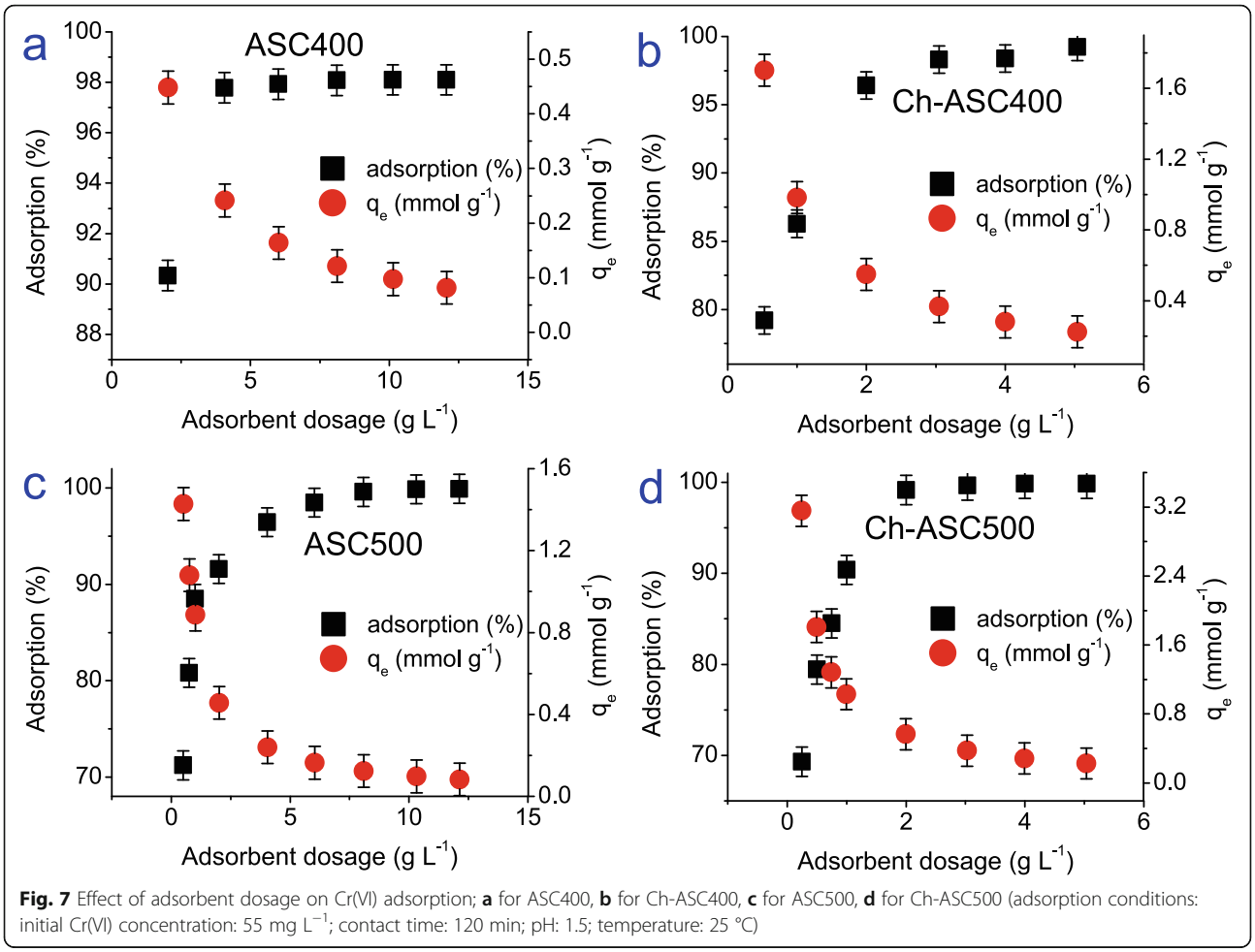

Fig. 7 Effect of adsorbent dosage on Cr(VI) adsorption; **a** for ASC400, **b** for Ch-ASC400, **c** for ASC500, **d** for Ch-ASC500 (adsorption conditions: initial Cr(VI) concentration: 55 mg L^{-1}; contact time: 120 min; pH: 1.5; temperature: 25 °C)

Zhang 2019). The fact that the R^2 values of the D-R model were found near 1 indicates the accuracy of the comments made with this model. R^2 values of Temkin isotherm were found close to 1 for all adsorbents. According to this model, the adsorptive heat of all molecules decreases linearly with the degree of coverage because of adsorbent-adsorbate interactions (Zhang et al. 2018).

The calculated maximum monolayer adsorption capacities (A_s) of ASC400, Ch-ASC400, ASC500 and Ch-ASC500 are 24.15 mg g^{-1} (0.4644 mmol g^{-1}), 54.95 mg g^{-1} (1.0569 mmol g^{-1}), 27.38 mg g^{-1} (0.5265 mmol g^{-1}), and 87.86 mg g^{-1} (1,6898 mmol g^{-1}), respectively. Increasing the pyrolysis temperature of the almond shell from 400 to 500 °C caused an increase of 13.4% in the adsorption capacity when the adsorbent was used in its raw form, and 59.9% when it was used as coated with chitosan. In addition, coating the adsorbents with chitosan increased their adsorption capacity by an average of 174%.

The maximum adsorption capacities of Cr(VI) obtained in some similar studies in the literature are given in Table 2.

Effect of contact time on Cr(VI) adsorption

The change of Cr(VI) adsorption percentages versus the change in contact time are given in the graph in Fig. 9 a and b. Due to the filling of available active sites on the adsorbent surface, the adsorption reached equilibrium after 120 minutes. For this reason, 120 minutes has been chosen as the optimum value. The equilibrium adsorption capacities (q_e) are as follows: 11.75 mg g^{-1} for ASC400, 37.82 mg g^{-1} for Ch-ASC400, 11.83 mg g^{-1} for ASC500, and 38.76 mg g^{-1} for Ch-ASC500.

Adsorption kinetics

Using the results of contact time experiments, the determination coefficients, rate constants, and model constants of the pseudo-first-order kinetic model, pseudo-second-order kinetic model, intra-particle diffusion model, and film diffusion model were calculated for the process. These values are given in Table 1.

According to the information in Table 1, if the pseudo-first-order and pseudo-second-order kinetic models are compared, since the determination coefficient values are greater and the calculated equilibrium

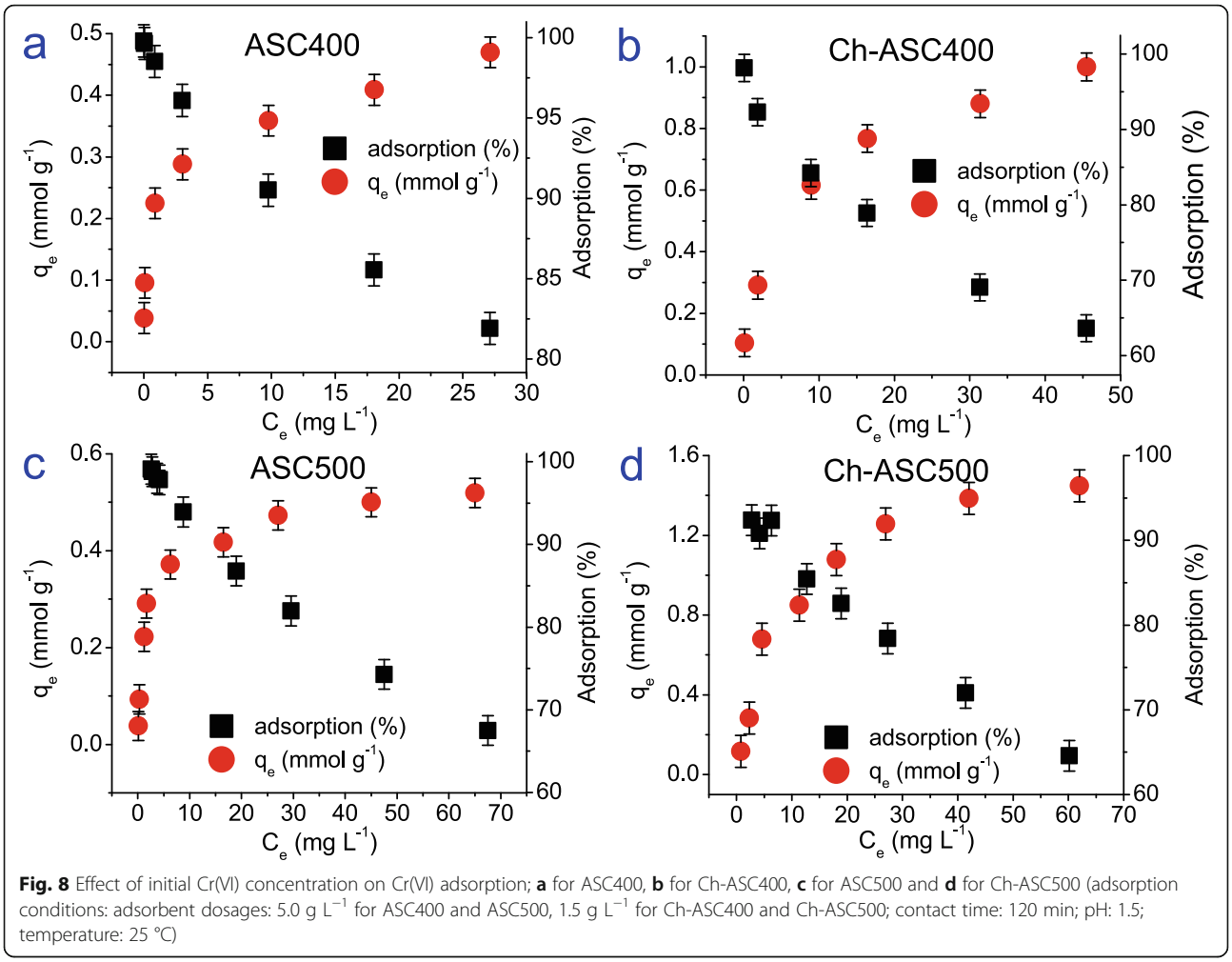

Fig. 8 Effect of initial Cr(VI) concentration on Cr(VI) adsorption; **a** for ASC400, **b** for Ch-ASC400, **c** for ASC500 and **d** for Ch-ASC500 (adsorption conditions: adsorbent dosages: 5.0 g L^{-1} for ASC400 and ASC500, 1.5 g L^{-1} for Ch-ASC400 and Ch-ASC500; contact time: 120 min; pH: 1.5; temperature: 25 °C)

adsorption capacities (q) are closer to the experimental equilibrium adsorption capacities (q_e) mentioned before, it is understood that the pseudo-second-order kinetic model is more compatible for adsorption kinetics. Therefore, chemical adsorption is probably more effective in the rate-determining step of the process (Sattar et al. 2019).

Intra-particle diffusion and film diffusion models were also applied to the adsorption data to analyze diffusion mechanisms. According to the intra-particle diffusion model, the adsorption process can be roughly divided into two sections (step 1 and step 2). The first section refers to the outer surface adsorption, the second section to the intra-particle diffusion of the adsorption. None of the linear graphs in both sections passes through the origin. This indicates that the adsorption process is not dominated solely by intra-particle diffusion (Ma et al. 2019). Film diffusion model graphics are linear and do not pass through the origin. This shows that film diffusion is also effective in the adsorption rate (Oussalah et al. 2019).

Effect of pH on Cr(VI) adsorption

In the graph showing the changes of Cr(VI) adsorption percentages versus the pH change given in Fig. 9 c and d, it is seen that the adsorption decreases as the pH of the solution increases. Accordingly, it can be interpreted that adsorption will be more efficient at acidic pHs.

Solution pH is a critical factor for the adsorption of Cr(VI), because the existing forms and redox potential of Cr(VI) ions in the solution and the surface charge of the adsorbent vary depending on the pH (Zhang et al. 2020).

Cr(VI) exists as different oxyanions depending on the solution pH. Among these oxyanions, the dominant species is $H_2CrO_4^-$ when pH < 1, $HCrO_4^-$ and $Cr_2O_7^{2-}$ when pH < 6.5, and CrO_4^{2-} when pH > 7.5 (Foroutan et al. 2018; Mei et al. 2019). In the pH range of 1 to 3, $HCrO_4^-$ is more abundant in the medium. Since the molar volume of $HCrO_4^-$ (44 cm^3 mol^{-1}) is smaller than the molar volume of $Cr_2O_7^{2-}$ (73 cm^3 mol^{-1}), the $HCrO_4^-$ oxyanion passes through the adsorbent layers and active sites more easily and adheres to them

Table 1 Isotherm, kinetic, diffusion, and thermodynamic parameters and determination coefficients

Models/parameters		ASC400	Ch-ASC400	ASC500	Ch-ASC500
Freundlich					
	K_F	2.8728	7.3672	3.3620	23.659
	N	3.0826	2.4643	2.7518	1.7646
	R^2	0.9582	0.9935	0.8840	0.9248
Langmuir					
	K_b	4306.2	1182.8	2374.0	538.00
	A_s (mmol g^{-1})	0.4644	1.0569	0.5265	1.6898
	R^2	0.9979	0.9857	0.9978	0.9955
Scatchard					
	K_s	21242	3144.9	4331.9	500.60
	Q_s (mmol g^{-1})	0.3883	0.8839	0.4865	1.7466
	R^2	0.7930	0.6841	0.9543	0.8604
D-R					
	X_m	0.7955	1.7727	1.0010	4.1421
	K	0.0030	0.0043	0.0040	0.0071
	E (kJ mol^{-1})	12.910	10.783	11.180	8.3918
	R^2	0.9877	0.9932	0.9468	0.9626
Temkin					
	b (J mol^{-1})	827.27	299.91	628.68	146.56
	A_T (L g^{-1})	68.106	7.3666	17.103	1.5026
	R^2	0.9832	0.9473	0.9883	0.9814
Pseudo-first-order model					
	K	0.0113	0.0334	0.0154	0.0180
	q (mmol g^{-1})	0.0289	0.4362	0.0275	0.3178
	R^2	0.9221	0.9734	0.9820	0.9903
Pseudo-second-order model					
	H	0.0701	0.0917	0.0864	0.0745
	K	1.3511	0.1612	1.6474	0.1245
	q (mmol g^{-1})	0.2278	0.7541	0.2291	0.7735
	R^2	0.9997	0.9995	0.9999	0.9996
Intra-particle diffusion model					
Step 1	K_i	0.0041	0.0480	0.0026	0.0385
	R^2	0.8035	0.9979	0.8866	0.9562
Step 2	K_i	0.0018	0.0107	0.0009	0.0088
	R^2	0.9996	0.7222	0.9994	0.9782
Film diffusion model					
	k_{fd}	0.0112	0.0334	0.0155	0.0179
	R^2	0.9221	0.9734	0.9820	0.9903
Thermodynamic parameters					
ΔH (kJ mol^{-1})		25.421	36.009	6.939	− 1.143
ΔS (J $K^{-1}mol^{-1}$)		109.71	149.52	52.64	23.73
ΔG (kJ mol^{-1})	298.15 K	− 7.288	− 8.569	− 8.756	− 8.219
	308.15 K	− 8.385	− 10.064	− 9.282	− 8.456
	318.15 K	− 9.482	− 11.559	− 9.809	− 8.635

Table 1 Isotherm, kinetic, diffusion, and thermodynamic parameters and determination coefficients *(Continued)*

Models/parameters	ASC400	Ch-ASC400	ASC500	Ch-ASC500
328.15 K	− 10.579	− 13.054	− 10.335	− 8.930
Temperature range in which adsorption is spontaneous	> − 41.4 °C	> − 32.3 °C	> − 141.3 °C	All temperatures

(Foroutan et al. 2018). In addition, at lower pH than the pH_{pzc} of the adsorbent, functional groups in the adsorbent structure are protonated (such as $-OH^+$, $-NH_2^+$) and the adsorbent surface is positively charged. Moreover, as the pH decreases, the number of positive charges on the adsorbent surface also increases. Thus, the positively charged adsorbent surface electrostatically attracts negatively charged Cr(VI) oxyanions. This is one of the reasons why adsorption is effective at low pH (Bahador et al. 2021; Yüksel and Orhan 2019). Another reaction that is probably effective in the adsorption process is as follows the non-protonated -OH groups on the adsorbent surface can donate an electron to Cr(VI) to reduce Cr(VI) to Cr(III). Cr(III) formed in this way is adsorbed by chelating reaction with $-NH_2$ groups, which are also non-protonated (Lu et al. 2017).

Effect of temperature on Cr(VI) adsorption

The change of adsorption percentage with temperature is given in Fig. 9 e and f. It can be seen that the percentage of adsorption varies slightly with temperature. For this reason, it can be said that adsorption is not affected by the temperature much.

Adsorption thermodynamics

The thermodynamic parameters of adsorption were calculated using the results of adsorption experiments at different temperatures. These parameters are given in Table 1. According to these data, the negative Gibbs free energy (ΔG) for all adsorbents indicates that the adsorption is spontaneous. When the enthalpy changes (ΔH) are examined, it is seen that adsorption is endothermic for ASC400, Ch-ASC400, and ASC500 adsorbents, while it is exothermic for Ch-ASC500. However, when the graph in Fig. 9f for Ch-ASC500 is examined and considering that the ΔH value in Table 1 is close to 0, it can be said that temperature has little effect on the adsorption. Finally, the entropy changes (ΔS) show that the irregularity at the adsorbent and solution interface decreases when ASC400 is used as the adsorbent and increases when other adsorbents are used (Kołodyńska et al. 2017).

Effect of the presence of Cl^-

Effect of 0.1 M and 0.2 M Cl^- ion to adsorption capacities under the optimum conditions is illustrated in Fig. 10. Accordingly, the presence of Cl^- ion reduced the adsorption capacity of adsorbents by 38 to 75%. Chitosan-coated adsorbents were more affected by the presence of this ion. Decreased efficiency with increasing the Cl^- content can be attributed to the occupation of active places in adsorbents (Foroutan et al. 2021).

Conclusion

Studies are carried out on various adsorbents for the removal of Cr(VI) from water by adsorption. In this study, it was aimed to synthesize a low-cost and effective

Table 2 The maximum adsorption capacities of Cr(VI) obtained in some similar studies

Adsorbent	Maximum Cr(VI) adsorption capacity (mg g^{-1})	Reference
Almond shell	3.40	(Pehlivan and Altun 2008)
Walnut shell	8.01	(Pehlivan and Altun 2008)
Hazelnut shell	8.28	(Pehlivan and Altun 2008)
Rice straw biochar-supported nanoscale zero-valent iron	40.00	(Qian et al. 2017)
Magnetic biochar prepared from *Melia azedarach* wood	25.27	(Zhang et al. 2018)
Pinewood sawdust/$Fe(NO_3)_3{\cdot}9H_2O$ magnetic biochar	42.70	(Yang et al. 2017)
Biochar derived from almond shell supported nano-zero-valent iron composite	26.63	(Shu et al. 2020)
Chitosan combined with magnetic loofah biochar	30.14	(Xiao et al. 2019)
$CaCl_2$-modified *Sargassum oligocystum* biomass	34.36	(Foroutan et al. 2018)
Ziziphus spina–christi leaf-activated carbon	13.81	(Abshirini et al. 2019)

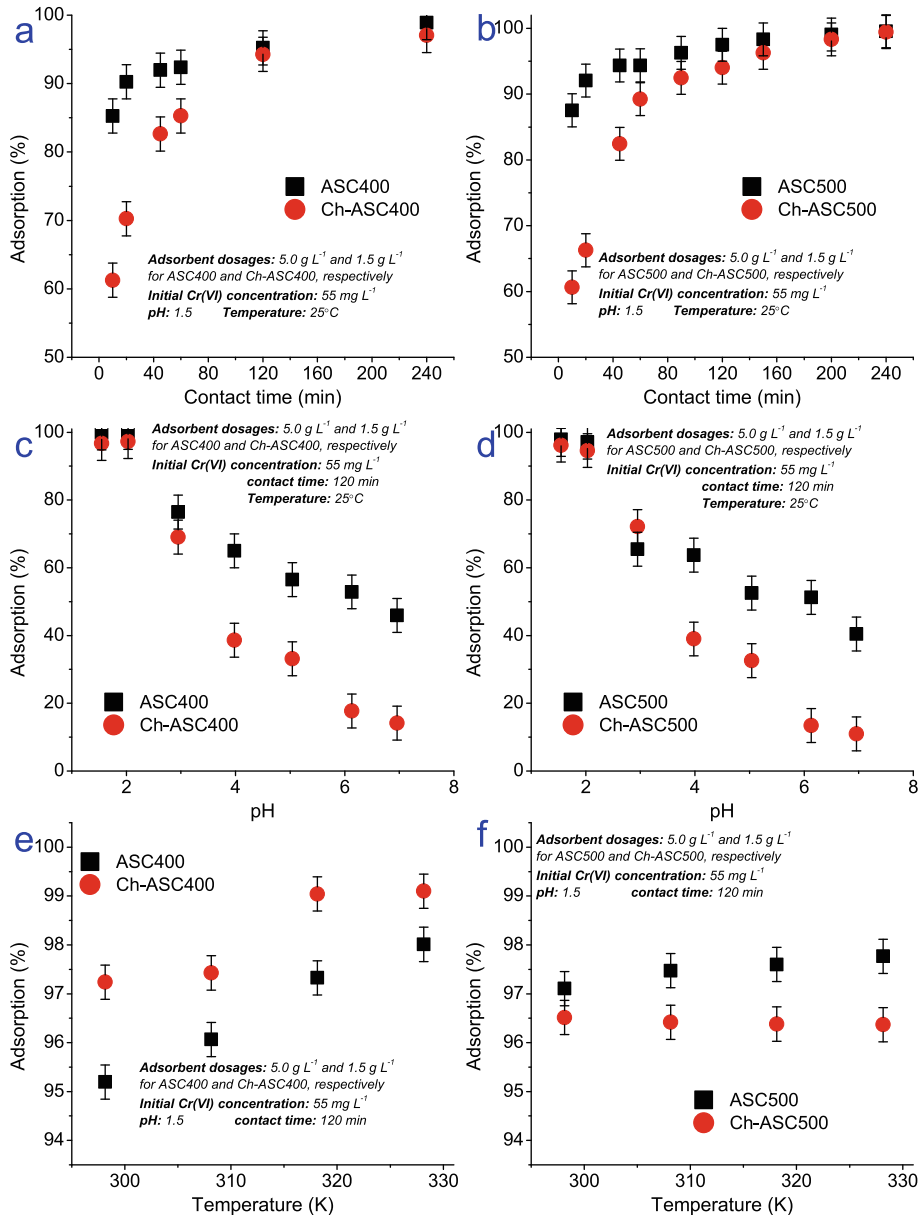

Fig. 9 Effect of contact time (**a** and **b**), pH (**c** and **d**), and temperature (**e** and **f**) on Cr(VI) adsorption: **a**, **c**, and **e** for ASC400 and Ch-ASC400; **b**, **d**, and **f** for ASC500 and Ch-ASC500

adsorbent and to elucidate the Cr(VI) adsorption mechanism. ASC400, ASC500, Ch-ASC400, and Ch-ASC500 adsorbents produced for this purpose were effective in the adsorption of Cr(VI). Increasing the pyrolysis temperature of the adsorbents and coating them with chitosan during the adsorbent synthesis stage increased their adsorption performance. Optimum operating conditions were determined as a result of the batch adsorption experiments. It has been observed that adsorption is more effective at acidic pHs, and temperature does not affect adsorption much. The equilibrium, kinetic, and thermodynamic properties of adsorption were investigated to elucidate the adsorption mechanism. At this stage, the compatibilities of the adsorption with the Langmuir isotherm and the pseudo-second-order kinetic model showed that the dominant mechanism is chemical adsorption. In addition, the adsorption energy values calculated with the D-R model supported this interpretation. It has been reported that both intra-particle and film diffusion are effective in adsorption. It was also seen in the study that adsorption is spontaneous for all adsorbents.

In addition, the adsorption performance of all adsorbents was found to be higher at low pH. Based on these

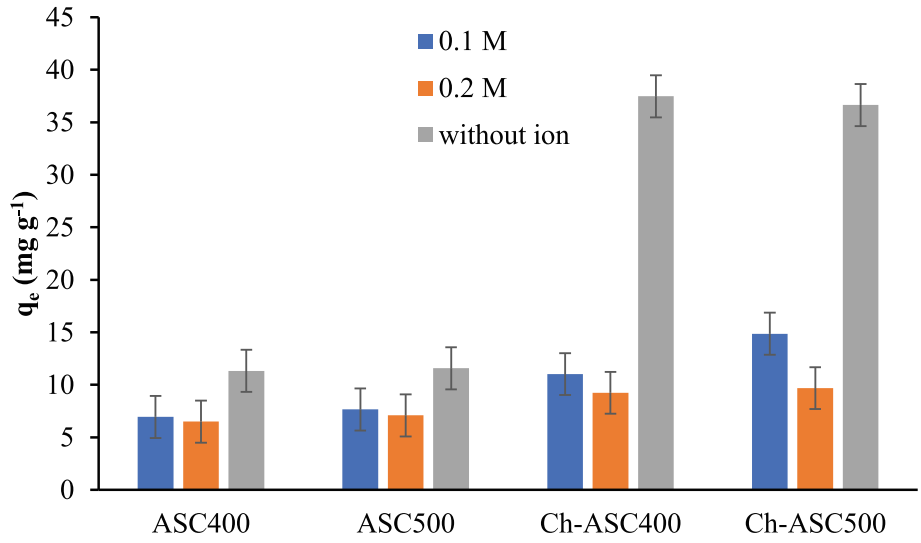

Fig. 10 Effect of presence of Cl^- (adsorption conditions: initial Cr(VI) concentration: 55 mg L^{-1}; contact time: 120 min; pH: 1.5; temperature: 25 °C)

results it has been interpreted that electrostatic attraction forces are predominant in the adsorption mechanism.

With the help of pH_{pzc}, FTIR, SEM, and EDX analyses, characterizations of adsorbents were revealed and it was proven that Cr(VI) was adsorbed.

Abbreviations

ASC400: Almond shell biochar (pyrolyzed at 400 °C); ASC500: Almond shell biochar (pyrolyzed at 500 °C); Ch-ASC400: Chitosan-coated almond shell biochar (pyrolyzed at 400 °C); Ch-ASC500: Chitosan-coated almond shell biochar (pyrolyzed at 500 °C); D-R: Dubinin-Radushkevich; FTIR: Fourier transform infrared spectroscopy; SEM: Scanning electron microscope; EDX: Energy dispersive X-ray; pH_{pzc}: The point of zero charge pH

Supplementary Information

The online version contains supplementary material available at https://doi.org/10.1186/s40543-021-00288-0.

Additional file 1:. Fig. A.1

Additional file 2:. Fig. A. 2

Acknowledgements

Not applicable

Authors' contributions

TA analyzed the data and interpreted the results. HE made adsorption experiments and characterization studies. YK obtained the biochars by pyrolyzing the almond shells. BÇ prepared adsorbents using biochars. All authors read and approved the final manuscript.

Availability of data and materials

The datasets used and/or analyzed during the current study are available from the corresponding author on reasonable request.

Declarations

Competing interests

The authors declare that they have no competing interests

Author details

[1]Department of Chemical Engineering, Konya Technical University, 42079 Konya, Turkey. [2]Department of Petroleum and Natural Gas Engineering, Iskenderun Technical University, 31200 Iskenderun, Hatay, Turkey. [3]Department of Chemical Engineering, Eskişehir Osmangazi University, 26480 Eskişehir, Turkey.

Received: 9 April 2021 Accepted: 26 July 2021
Published online: 19 August 2021

References

Abshirini Y, Foroutan R, Esmaeili H. Cr(VI) removal from aqueous solution using activated carbon prepared from *Ziziphus spina–christi* leaf. Materials Research Express. 2019;6:(4).

Ahsaine HA, Zbair M, Anfar Z, Naciri Y, el Alem N, Ezahri M. Cationic dyes adsorption onto high surface area 'almond shell' activated carbon: kinetics, equilibrium isotherms and surface statistical modeling. Materials Today Chemistry. 2018;8:121–32. https://doi.org/10.1016/j.mtchem.2018.03.004.

Altun T. Chitosan-coated sour cherry kernel shell beads: an adsorbent for removal of Cr (VI) from acidic solutions. Journal of Analytical Science and Technology. 2019;10(1):14. https://doi.org/10.1186/s40543-019-0172-6.

Altun T, Ecevit H. Cr (VI) removal using Fe 2 O 3-chitosan-cherry kernel shell pyrolytic charcoal composite beads. Environmental Engineering Research. 2020;25(3):426–38.

Bahador F, Foroutan R, Esmaeili H, Ramavandi B. Enhancement of the chromium removal behavior of Moringa oleifera activated carbon by chitosan and iron oxide nanoparticles from water. Carbohydr Polym. 2021 Jan;251:117085. https://doi.org/10.1016/j.carbpol.2020.117085.

Banerjee M, Bar N, Basu RK, Das SK. Comparative study of adsorptive removal of Cr (VI) ion from aqueous solution in fixed bed column by peanut shell and almond shell using empirical models and ANN. Environ Sci Pollut Res. 2017; 24(11):10604–20. https://doi.org/10.1007/s11356-017-8582-8.

Brion-Roby R, Gagnon J, Deschênes J-S, Chabot B. Development and treatment procedure of arsenic-contaminated water using a new and green chitosan sorbent: kinetic, isotherm, thermodynamic and dynamic studies. Pure Appl Chem. 2018;90(1):63–77. https://doi.org/10.1515/pac-2017-0305.

Dandil S, Akin Sahbaz D, Acikgoz C. Adsorption of Cu(II) ions onto crosslinked chitosan/Waste Active Sludge Char (WASC) beads: Kinetic, equilibrium, and thermodynamic study. Int J Biol Macromol. Elsevier B.V.; 2019 Sep 1;136:668–675.

Dewage NB, Fowler RE, Pittman CU, Mohan D, Mlsna T. Lead (Pb 2+) sorptive removal using chitosan-modified biochar: batch and fixed-bed studies. RSC Adv. 2018;8(45):25368–77. https://doi.org/10.1039/C8RA04600J.

Duran C, Ozdes D, Gundogdu A, Senturk HB. Kinetics and isotherm analysis of basic dyes adsorption onto almond shell (Prunus dulcis) as a low cost

adsorbent. J Chem Eng Data. 2011;56(5):2136–47. https://doi.org/10.1021/je101204j.
Esvandi Z, Foroutan R, Peighambardoust SJ, Akbari A, Ramavandi B. Uptake of anionic and cationic dyes from water using natural clay and clay/starch/MnFe2O4 magnetic nanocomposite. Surfaces and Interfaces. 2020 Dec;21:100754. https://doi.org/10.1016/j.surfin.2020.100754.
Foroutan R, Mohammadi R, Ramavandi B. Treatment of chromium-laden aqueous solution using CaCl2-modified Sargassum oligocystum biomass: characteristics, equilibrium, kinetic, and thermodynamic studies. Korean J Chem Eng. 2018;35:(1).
Foroutan R, Peighambardoust SJ, Mohammadi R, Omidvar M, Sorial GA, Ramavandi B. Influence of chitosan and magnetic iron nanoparticles on chromium adsorption behavior of natural clay: Adaptive neuro-fuzzy inference modeling. Int J Biol Macromol. 2020 May;151:355–65. https://doi.org/10.1016/j.ijbiomac.2020.02.202.
Foroutan R, Peighambardoust SJ, Ahmadi A, Akbari A, Farjadfard S, Ramavandi B. Adsorption mercury, cobalt, and nickel with a reclaimable and magnetic composite of hydroxyapatite/Fe3O4/polydopamine. Journal of Environmental Chemical Engineering. 2021 Aug;9:4.
Freundlich H. Über die adsorption in lösungen. Z Phys Chem. 1907;57(1):385–470.
Hu Q, Zhang Z. Application of Dubinin–Radushkevich isotherm model at the solid/solution interface: A theoretical analysis. Journal of Molecular Liquids [Internet]. 2019;277:646–8. Available from: https://www.sciencedirect.com/science/article/pii/S0167732218346087. https://doi.org/10.1016/j.molliq.2019.01.005.
Imran M, Khan ZUH, Iqbal MM, Iqbal J, Shah NS, Munawar S, et al. Effect of biochar modified with magnetite nanoparticles and HNO3 for efficient removal of Cr (VI) from contaminated water: a batch and column scale study. Environ Pollut. 2020;261:114231. https://doi.org/10.1016/j.envpol.2020.114231.
Kołodyńska D, Bąk J, Kozioł M, Pylychuk L. Investigations of heavy metal ion sorption using nanocomposites of iron-modified biochar. Nanoscale Res Lett. 2017;12(1):433.
Langmuir I. The constitution and fundamental properties of solids and liquids. Part I. Solids. J Am Chem Soc. 1916;38(11):2221–95. https://doi.org/10.1021/ja02268a002.
Liu S, Huang B, Chai L, Liu Y, Zeng G, Wang X, et al. Enhancement of As (V) adsorption from aqueous solution by a magnetic chitosan/biochar composite. RSC Adv. 2017;7(18):10891–900. https://doi.org/10.1039/C6RA27341F.
Lu J, Xu K, Yang J, Hao Y, Cheng F. Nano iron oxide impregnated in chitosan bead as a highly efficient sorbent for Cr (VI) removal from water. Carbohydr Polym. 2017;173:28–36. https://doi.org/10.1016/j.carbpol.2017.05.070.
Ma H, Yang J, Gao X, Liu Z, Liu X, Xu Z. Removal of chromium (VI) from water by porous carbon derived from corn straw: influencing factors, regeneration and mechanism. J Hazard Mater. 2019;369:550–60. https://doi.org/10.1016/j.jhazmat.2019.02.063.
Mei J, Zhang H, Li Z, Ou H. A novel tetraethylenepentamine crosslinked chitosan oligosaccharide hydrogel for total adsorption of Cr (VI). Carbohydr Polym. 2019;224:115154. https://doi.org/10.1016/j.carbpol.2019.115154.
Oussalah A, Boukerroui A, Aichour A, Djellouli B. Cationic and anionic dyes removal by low-cost hybrid alginate/natural bentonite composite beads: adsorption and reusability studies. Int J Biol Macromol. 2019;124:854–62. https://doi.org/10.1016/j.ijbiomac.2018.11.197.
Parlayıcı Ş. Modified peach stone shell powder for the removal of Cr (VI) from aqueous solution: synthesis, kinetic, thermodynamic, and modeling study. International journal of phytoremediation. 2019;21(6):590–9. https://doi.org/10.1080/15226514.2018.1540541.
Pehlivan E, Altun T. Biosorption of chromium (VI) ion from aqueous solutions using walnut, hazelnut and almond shell. J Hazard Mater. 2008;155(1–2):378–84. https://doi.org/10.1016/j.jhazmat.2007.11.071.
Peng H, Guo J. Removal of chromium from wastewater by membrane filtration, chemical precipitation, ion exchange, adsorption electrocoagulation, electrochemical reduction, electrodialysis, electrodeionization, photocatalysis and nanotechnology: a review. Environ Chem Lett. 2020:1–14.
Qian L, Zhang W, Yan J, Han L, Chen Y, Ouyang D, et al. Nanoscale zero-valent iron supported by biochars produced at different temperatures: Synthesis mechanism and effect on Cr (VI) removal. Environ Pollut. 2017;223:153–60. https://doi.org/10.1016/j.envpol.2016.12.077.
Rai MK, Giri BS, Nath Y, Bajaj H, Soni S, Singh RP, et al. Adsorption of hexavalent chromium from aqueous solution by activated carbon prepared from almond shell: kinetics, equilibrium and thermodynamics study. J Water Supply Res Technol AQUA. 2018;67(8):724–37. https://doi.org/10.2166/aqua.2018.047.
Sargın İ, Arslan G. Chitosan/sporopollenin microcapsules: preparation, characterisation and application in heavy metal removal. Int J Biol Macromol. 2015;75:230–8. https://doi.org/10.1016/j.ijbiomac.2015.01.039.
Sargın I, Kaya M, Arslan G, Baran T, Ceter T. Preparation and characterisation of biodegradable pollen–chitosan microcapsules and its application in heavy metal removal. Bioresour Technol. 2015;177:1–7. https://doi.org/10.1016/j.biortech.2014.11.067.
Sattar MS, Shakoor MB, Ali S, Rizwan M, Niazi NK, Jilani A. Comparative efficiency of peanut shell and peanut shell biochar for removal of arsenic from water. Environ Sci Pollut Res. 2019;26(18):18624–35. https://doi.org/10.1007/s11356-019-05185-z.
Shu Y, Ji B, Cui B, Shi Y, Wang J, Hu M, et al. Almond shell-derived, biochar-supported, nano-zero-valent iron composite for aqueous hexavalent chromium removal: performance and mechanisms. Nanomaterials. 2020;10(2):198. https://doi.org/10.3390/nano10020198.
Stoia M, Muntean C, Militaru B. MnFe2O4 nanoparticles as new catalyst for oxidative degradation of phenol by peroxydisulfate. J Environ Sci. 2017;53:269–77. https://doi.org/10.1016/j.jes.2015.10.035.
Xiao F, Cheng J, Cao W, Yang C, Chen J, Luo Z. Removal of heavy metals from aqueous solution using chitosan-combined magnetic biochars. J Colloid Interface Sci. 2019;540:579–84. https://doi.org/10.1016/j.jcis.2019.01.068.
Yang P, Guo D, Chen Z, Cui B, Xiao B, Liu S, et al. Removal of Cr (VI) from aqueous solution using magnetic biochar synthesized by a single step method. J Dispers Sci Technol. 2017;38(11):1665–74. https://doi.org/10.1080/01932691.2016.1272058.
Yüksel Ş, Orhan R. The removal of Cr (VI) from aqueous solution by activated carbon prepared from apricot, peach stone and almond shell mixture in a fixed-bed column. Arab J Sci Eng. 2019;44(6):5345–57. https://doi.org/10.1007/s13369-018-3618-z.
Zhang X, Lv L, Qin Y, Xu M, Jia X, Chen Z. Removal of aqueous Cr (VI) by a magnetic biochar derived from Melia azedarach wood. Bioresour Technol. 2018;256:1–10. https://doi.org/10.1016/j.biortech.2018.01.145.
Zhang H, Xiao R, Li R, Ali A, Chen A, Zhang Z. Enhanced aqueous Cr (VI) removal using chitosan-modified magnetic biochars derived from bamboo residues. Chemosphere. 2020;127694.

Publisher's Note

Springer Nature remains neutral with regard to jurisdictional claims in published maps and institutional affiliations.

Submit your manuscript to a SpringerOpen journal and benefit from:

► Convenient online submission
► Rigorous peer review
► Open access: articles freely available online
► High visibility within the field
► Retaining the copyright to your article

Submit your next manuscript at ► springeropen.com